Bifurcation phenomena and control for magnetohydrodynamic flows in a smooth expanded channel*

G. C. Layek[a], Mani Shankar Mandal[b]†, and H. A. Khalaf[c]

[a] Department of Mathematics, The University of Burdwan, Burdwan 713104, India
[b] Department of Mathematics, Krishnagar Govt. College, Krishnagar, Nadia 741101, India
[c] Thi-Qar University, Marshes Research Center, Thi-Qar, Iraq

(Received 16 January 2014; revised manuscript received 17 April 2014; published online 24 September 2014)

This work reports the effects of magnetic field on an electrically conducting fluid with low electrical conductivity flowing in a smooth expanded channel. The governing nonlinear magnetohydrodynamic (MHD) equations in induction-free situations are derived in the framework of MHD approximations and solved numerically using the finite-difference technique. The critical values of Reynolds number (based on upstream mean velocity and channel height) for symmetry breaking bifurcation for a sudden expansion channel (1:4) is about 36, whereas the value in the case of the smooth expansion geometry used in this work is obtained as 298, approximately (non-magnetic case). The flow of an electrically conducting fluid in the presence of an externally applied constant magnetic field perpendicular to the plane of the flow is reduced significantly depending on the magnetic parameter (M). It is found that the critical value of Reynolds number for smooth expansion (1:4) is about 475 for the magnetic parameter $M = 2$. The separating regions developed behind the smooth symmetric expansion are decreased in length for increasing values of the magnetic parameter. The bifurcation diagram is shown for a symmetric smoothly expanding channel. It is noted that the critical values of Reynolds number increase with increasing magnetic field strength.

Keywords: weakly electrically conducting fluid, flow bifurcation, asymmetric flow, smooth expansion

PACS: 47.15.–x, 47.85.L–, 47.85.–g **DOI:** 10.1088/1674-1056/23/11/114701

1. Introduction

Substantial developments have been made in understanding the transitional regime for simple planar geometry, e.g. suddenly expanding channel, circular cylinder, pipe flow, etc. The symmetric flow field becomes unstable once the flow Reynolds number exceeds a critical value. With further increase of Reynolds number, the flow field becomes oscillatory. The flow dynamics in simple geometry is interesting and fundamentally important for understanding the physics of flow. Moreover, the prediction of the flow separation regions, multiple recirculating regions and flow bifurcation phenomena are crucial in many engineering flow devices.

The flow through a symmetric suddenly expanding channel has been demonstrated experimentally by Armaly *et al.*[1] and Durst *et al.*,[2,3] and numerically by Cherdron *et al.*,[4] Fearn *et al.*,[5] Drikakis[6] and many others. They made a significant contribution to understanding the channel flow with sudden symmetric expansion. The appearance of asymmetric flow with increase in Reynolds number in a symmetrical channel has been explained. The phenomenon is analyzed in terms of the Coanda effect by Wille and Fernholz.[7] The causes of instability have been studied by several authors, e.g. Sobey and Drazin,[8] Borgas and Pedley[9] and Shapira *et al.*[10] This symmetric flow structure first undergoes bifurcation leading to asymmetric flow structure (known as symmetry-breaking flow bifurcation) when the Reynolds number attains a critical value. On the other hand, bifurcation phenomena in viscoelastic fluids through (1:4) symmetric planar expansion geometries have been studied by Rocha *et al.*[11] The control of separating regions and flow bifurcation are of paramount importance from an engineering applications point of view. There are several separation controlling devices available, e.g. (i) construction of a streamline shaped body, (ii) application of suction through a porous boundary, (iii) embedding a solid block in the flow domain, (iv) application of electro-magnetic force in the case of an electrically conducting fluid in the presence of magnetic field, (v) viscoelastic force, (vi) inhomogeneity of fluid and others. The application of electromagnetic force in controlling the flow quantities has attracted the interest of many fluid mechanists because of the fact that the control of flow separation phenomena and instabilities plays a deciding role in the performance of fluid flow devices (e.g. Gad-el-Hak and Bushnell,[12] Bhattacharyya and Layek,[13] Bhattacharyya *et al.*,[14] Bhattacharyya *et al.*,[15] Nadeem and Haq,[16] Nadeem *et al.*[17]) The MHD principle is a method for affecting the flow field in a desired direction by altering the structure of the flow. Midya *et al.*,[18] Bandyopadhyay and Layek[19] and Layek and Midya[20] have studied extensively MHD flow in a channel with local constrictions and a backward step channel. They have shown that the regions of flow separation and

*Project support by the UGC (SAP), DSA-I in the Mathematics Department, Burdwan University, India.
†Corresponding author. E-mail: manimath@yahoo.com
© 2014 Chinese Physical Society and IOP Publishing Ltd

bifurcation can be controlled using a suitable value of magnetic field strength. It was shown by Holstein *et al.*[21] that self-similar boundary layer flow without separation is possible in a divergent channel when the suction strength K satisfies $K \geq 2\sqrt{2}$. MHD boundary layer flow without separation in a diverging channel with non-porous walls is possible if the strength of the magnetic field is greater than two.[22] Recently, Layek *et al.*[23] have shown that MHD boundary layer flow in a diverging channel is possible even in the presence of blowing at the walls provided that the strength of the magnetic field is greater than two. The MHD boundary layer flows for different types of fluid model have been studied extensively for the last 100 years (see, e.g., Nadeem *et al.*,[24] Nadeem *et al.*,[25] Akbar *et al.*,[26] Nadeem *et al.*,[27] Bhattacharyya and Layek,[28] Bhattacharyya and Layek[29]).

The aim of the present study is to report the MHD flow of an electrically conducting fluid in the presence of uniform externally applied magnetic field through a smooth symmetric expanded channel. In this analysis, we have neglected the induced field for the flow of liquid metals with very low electrical conductivities. This assumption is valid for most laboratory and technical flows of liquid metals since the magnetic Reynolds number is usually very small (e.g. 10^{-5} for sodium and 10^{-7} for mercury). The analysis reveals that the lengths of separation diminish with increasing values of the magnetic parameter and suppress the symmetry-breaking flow bifurcation for the flow of an electrically conducting fluid through a symmetric smoothly expanding channel. The bifurcation is supercritical for the increase of the magnetic parameter.

2. Formulation of the flow problem

We consider a two-dimensional laminar iso-thermal motion of an electrically conducting incompressible viscous fluid (flows of liquid metals) with electrical conductivity σ flowing in a smoothly expanding channel in the presence of static magnetic field B_0 in the direction of the y^* axis (see Fig. 1 for geometrical sketch and physical flow configuration). The magnetic permeability ($\mu_{\rm m}$) is considered to be constant in the conducting medium. Let (x^*, y^*) be the Cartesian co-ordinate of a material point in the system such that the x^* axis is along the lower wall and the y^* axis is perpendicular to it. Let (u^*, v^*) be the velocity components along the x^* and y^* directions, respectively; p^* is the pressure and U is the mean velocity at the inlet section of the channel. The electric current is generated in the normal to the plane of flow. The induced magnetic field is negligible compared with the imposed field for low electrical conductivity liquid. The flow problem is solved in the induction-less situation. Therefore, the total magnetic field is simply given by the applied magnetic field B_0. This approximation is valid when the magnetic Reynolds number $\mathrm{R_M}$ ($\mu_{\rm m}\sigma hU \ll 1$) is less than one. In other words, the magnetic diffusion time is much smaller than other time scales. In the case of liquid metals, the value of $R_{\rm M}$ is usually less than 10^{-2}. In laboratory or industrial flows of liquid metals, where the magnetic Reynolds number is normally very small, the effect of the Lorentz force reduces to Joule dissipation, which suppresses the three-dimensional motions. This problem may be useful for construction of liquid metal cooling blankets for fusion reactors or for optimization of processes of semiconductor crystal growth or continuous casting of metals (magnetic braking).[30] In the case of blood flow in the left coronary artery the magnetic Reynolds number is 0.02, taking the electrical conductivity of the flowing blood $\sigma = 6 \times 10^{-1}$ mho·m^{-1} with arterial radius 3.75×10^{-3} m and velocity 8.8 m·h^{-1}.[18] For liquid mercury the electrical conductivity is 10^{-5} e.m.u and for liquid sodium 10^{-4} e.m.u. It is also assumed that the external electric field is zero and the electric field due to polarization of charges is negligible.

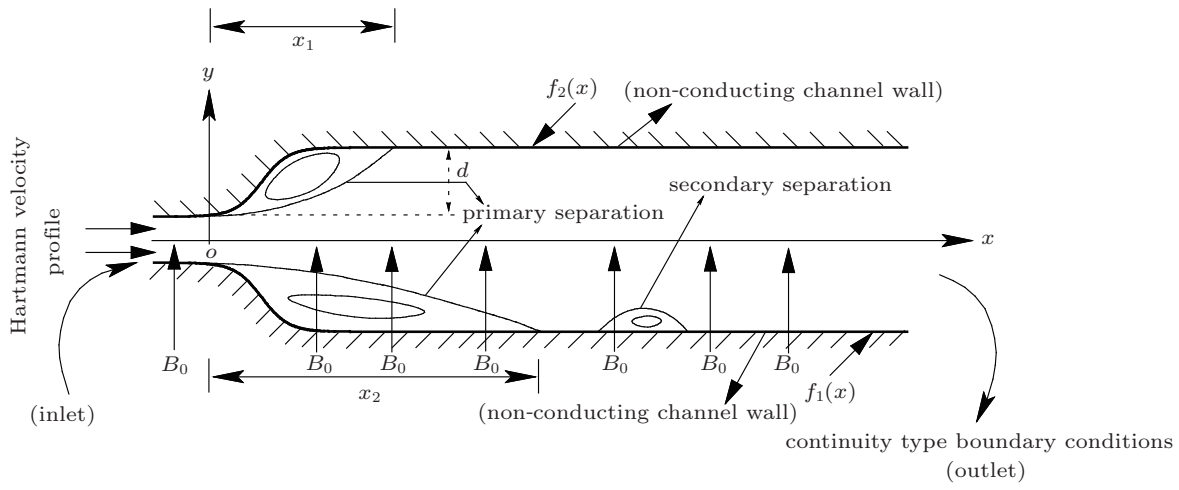


Fig. 1. Sketch of the smoothly expanding channel depicting the co-ordinates and the asymmetric flow structure.

The Navier–Stokes equations of motion for an incompressible electrically conducting viscous fluid taking into account the electro-magnetic force known as Lorentz force under MHD approximations may be written in dimensionless form as

$$\frac{\partial u}{\partial t}+u\frac{\partial u}{\partial x}+v\frac{\partial u}{\partial y}=-\frac{\partial p}{\partial x}+\frac{1}{Re}\left(\frac{\partial^2 u}{\partial x^2}+\frac{\partial^2 u}{\partial y^2}\right)-\frac{M^2}{Re}u, \quad (1)$$

$$\frac{\partial v}{\partial t}+u\frac{\partial v}{\partial x}+v\frac{\partial v}{\partial y}=-\frac{\partial p}{\partial y}+\frac{1}{Re}\left(\frac{\partial^2 v}{\partial x^2}+\frac{\partial^2 v}{\partial y^2}\right), \quad (2)$$

$$\frac{\partial u}{\partial x}+\frac{\partial v}{\partial y}=0. \quad (3)$$

The following non-dimensional variables are used:

$$x=x^*/h,\quad y=y^*/h,\quad u=u^*/U,\quad v=v^*/U,$$
$$p=p^*/(\rho U^2),\quad t=(t^*U)/h. \quad (4)$$

The dimensionless parameters $Re(=Uh/\upsilon)$ and $M(=B_0h\sqrt{\sigma/\rho\upsilon})$ are the Reynolds and Hartmann numbers (proportional to the strength of magnetic field B_0). The Lorentz force $\left(\boldsymbol{J}\times\boldsymbol{B}=-(M^2/Re)u\right)$ acts on the flow field, $\boldsymbol{J}\,(=\boldsymbol{\nabla}\times\boldsymbol{H})$ being the current density vector.

Now, we define the dimensionless stream function $\psi(x,y,t)$ and the vorticity function $\omega(x,y,t)$ in this two-dimensional flow as

$$u=\frac{\partial\psi}{\partial y},\quad v=-\frac{\partial\psi}{\partial x},\quad -\omega=\left(\frac{\partial u}{\partial y}-\frac{\partial v}{\partial x}\right). \quad (5)$$

Using Eq. (5) and by cross-differentiation of the momentum equations (1) and (2) the pressure term is completely eliminated and we have the following coupled equations for stream function and vorticity:

$$\frac{\partial^2\psi}{\partial x^2}+\frac{\partial^2\psi}{\partial y^2}=-\omega, \quad (6)$$

$$\frac{\partial\omega}{\partial t}+\frac{\partial\psi}{\partial y}\frac{\partial\omega}{\partial x}-\frac{\partial\psi}{\partial x}\frac{\partial\omega}{\partial y}=\frac{1}{Re}\left(\frac{\partial^2\omega}{\partial x^2}+\frac{\partial^2\omega}{\partial y^2}\right)+\frac{M^2}{Re}\frac{\partial u}{\partial y}. \quad (7)$$

The boundary conditions of the flow problem are given as follows.

The streamwise and transverse velocity components should be zero at the rigid walls (no-slip condition). At the inlet section of the channel the fully developed Hartmann flow is prescribed (Ref. [31]). The boundary condition at the outlet cross-section of the channel is taken as a continuity type. This gives the conditions as

$$\frac{\partial^2\psi}{\partial x^2}=\frac{\partial^2\omega}{\partial x^2}=0$$

at the outlet.

The channel walls are assumed to be electrically non-conducting.

2.1. Shape of smoothly expanding channel

In this study, the channel walls are electrically non-conducting as in the Hartmann flow problem. Therefore, the non-conducting lower and upper walls of the channel are represented mathematically as (see Ref. [32])

$$f_1(x)=-\frac{d}{2}\tanh\left(\frac{x}{d}\right),\ f_2(x)=1+\frac{d}{2}\tanh\left(\frac{x}{d}\right). \quad (8)$$

Here d is a parameter representing the height of the smooth expansion of the channel (shown in Fig. 1).

2.2. Solution of Hartmann flow

The equation of motion for uni-directional flow (balance of streamwise pressure gradient, magnetic force, and viscous stress) can be written as

$$-\frac{\partial p^*}{\partial x^*}+\rho\upsilon\frac{\mathrm{d}^2u^*}{\mathrm{d}y^{*2}}-j_zB_0=0, \quad (9)$$

where $u^*(y^*)$ is the velocity component of the uni-directional flow parallel to the channel walls (sketched in Fig. 1). Here the notation "$*$" indicates dimensional quantities. Electric current flows normal to the plane of flow and Ohm's law gives the current density j_z as

$$j_z=\sigma(E_z+u^*B_0). \quad (10)$$

The electric field E_z is constant because $\boldsymbol{\nabla}\times\boldsymbol{E}=0$ in the steady flow. Since the physical variables apart from pressure are functions of y^* only, it follows from Eq. (9) that $(\partial p^*/\partial x^*)=$ constant and this external pressure gradient is needed to drive the flow against viscous stress and the magnetic force (retarding effects).

Eliminating j_z between Eqs. (9) and (10) gives on using dimension-less variables equation (4)

$$\frac{\mathrm{d}^2u}{\mathrm{d}y^2}-M^2u=-\frac{h^2}{\rho\upsilon U}\left(\frac{\partial p^*}{\partial x^*}+\sigma E_zB_0\right), \quad (11)$$

where $u(y)=u^*(y^*)/U$.

The solution of Eq. (11) satisfying the conditions $u=0$ at $y=0$ and $u=0$ at $y=1$ gives the Hartmann velocity distribution as

$$u(y)=\frac{\cosh\left(\frac{M}{2}\right)-\cosh\left(\mathrm{M}\left(y-\frac{1}{2}\right)\right)}{8\sinh^2\left(\frac{\mathrm{M}}{4}\right)}, \quad (12)$$

with the relation

$$\frac{h^2}{\rho\upsilon U}\left(\frac{\partial p^*}{\partial x^*}+\sigma E_zB_0\right)=\frac{M^2\cosh\frac{M}{2}}{8\sinh^2\frac{M}{4}}. \quad (13)$$

Further flow rate Q in the channel is assumed constant. Thus, we obtain

$$Uh\int_0^1 u\,\mathrm{d}y=Q=\text{constant}, \quad (14)$$

which gives from Eq. (12) as

$$\frac{h}{8\sinh^2\frac{M}{4}}\left(\cosh\frac{M}{2}-\frac{2}{M}\sinh\frac{M}{2}\right)=\frac{Q}{U}. \tag{15}$$

Elimination of U from Eqs. (13) and (15) gives the external pressure gradient $(-\partial p^*/\partial x^*)$ as

$$-\frac{\partial p^*}{\partial x^*}=\frac{\rho\upsilon QM^3}{h^3\left(2\tanh\frac{M}{2}-M\right)}+\sigma E_z B_0. \tag{16}$$

It can be found from Eq. (16) that, to maintain a constant flow rate Q, the external pressure gradient is a function of the Hartmann number M.

It may further be noted that, under an electrically short-circuited condition, there is a non-zero net electric current normal to the plane of the flow since all the current flows in one direction. This can be seen from Eq. (10) with $E_z=0$. In fact,

$$\int_0^h j_z\,\mathrm{d}y^*=\sigma B_0\int_0^h u^*\,\mathrm{d}y^*, \tag{17}$$

which gives upon using Eq. (14) the net current normal to the plane of flow as in Ref. [18] ($\sigma B_0 Q$). We can assume the fully developed velocity component $u(y)$ given by Eq. (12) and $v=0$.

3. Transformation of the governing equations

A suitable co-ordinate transformation is considered, which makes the expanded channel into a rectangular geometry in the transformed plane. The transformations (for details see Layek and Midya[33]) are given by

$$\xi=x,\quad \eta=\frac{y-f_1(x)}{f_2(x)-f_1(x)}. \tag{18}$$

The transformed equations can be written in new co-ordinates (ξ,η) as

$$\begin{aligned}&\frac{\partial^2\psi}{\partial\xi^2}-(\mathcal{A}(\xi,\eta)-2\mathcal{B}(\xi,\eta)\mathcal{H}(\xi,\eta))\frac{\partial\psi}{\partial\eta}\\&-2\mathcal{B}(\xi,\eta)\frac{\partial^2\psi}{\partial\xi\partial\eta}+\left(\mathcal{B}^2(\xi,\eta)+\mathcal{G}^2(\xi)\right)\frac{\partial^2\psi}{\partial\eta^2}=-\omega, \quad (19)\\&\frac{\partial\omega}{\partial t}-u\left(\frac{\partial\omega}{\partial\xi}-\mathcal{B}(\xi,\eta)\frac{\partial\omega}{\partial\eta}\right)+v\mathcal{G}(\xi)\frac{\partial\omega}{\partial\eta}\\&=\frac{1}{Re}\left[\frac{\partial^2\omega}{\partial\xi^2}-(\mathcal{A}(\xi,\eta)-2\mathcal{B}(\xi,\eta)\mathcal{H}(\xi,\eta))\frac{\partial\omega}{\partial\eta}\right.\\&\left.-2\mathcal{B}(\xi,\eta)\frac{\partial^2\omega}{\partial\xi\partial\eta}+\left(\mathcal{B}^2(\xi,\eta)+\mathcal{G}^2(\xi)\right)\frac{\partial^2\omega}{\partial\eta^2}\right]\\&+\frac{M^2\mathcal{G}^2(\xi)}{Re}\frac{\partial^2\psi}{\partial\eta^2}. \quad (20)\end{aligned}$$

Here, $\mathcal{A}(\xi,\eta)$, $\mathcal{B}(\xi,\eta)$, $\mathcal{H}(\xi,\eta)$, and $\mathcal{G}(\xi)$ are some functions of ξ and η (for details see Ref. [19]).

4. Numerical solution procedure

The transformed governing equations together with the prescribed initial and boundary conditions are solved numerically by using the finite-difference technique. The alternating direction implicit (ADI) technique has been used to solve the vorticity transport equation. The elliptic stream function equation is discretized using the central difference formula and the obtained algebraic system is solved using the SLOR (successive line over-relaxation) algorithm.[34]

The finite-difference representations of the derivatives and all other terms have been written at the mesh point (j,k) in the computational plane, which indicates a point where $x=j\Delta\xi$, $y=k\Delta\eta$, and $t=m\Delta t$, with $\Delta\xi$, $\Delta\eta$, and Δt being the increments of ξ, η, and t respectively. The superscript denotes the time direction. A tri-diagonal system of algebraic equations associated with each line (constant j) in the η-direction is obtained. The finite-difference representation of Eq. (17) is given below.

$$a(k)\psi_{j,k-1}^{m+1}+b(k)\psi_{j,k}^{m+1}+c(k)\psi_{j,k+1}^{m+1}=s(k), \tag{21}$$

where the quantities $a(k)$, $b(k)$, $c(k)$, and $s(k)$ are constants and are given by

$$\begin{aligned}a(k)&=\frac{(\mathcal{A}-2\mathcal{B}\mathcal{H})}{2\Delta\eta}+\frac{(\mathcal{B}^2+\mathcal{G}^2)}{\Delta\eta^2},\\b(k)&=-\frac{2}{\Delta\xi^2}-\frac{2(\mathcal{B}^2+\mathcal{G}^2)}{\Delta\eta^2},\\c(k)&=-\frac{(\mathcal{A}-2\mathcal{B}\mathcal{H})}{2\Delta\eta}+\frac{(\mathcal{B}^2+\mathcal{G}^2)}{\Delta\eta^2},\\s(k)&=-\omega_{j,k}^m-\frac{\psi_{j+1,k}^m-2\psi_{j,k}^m+\psi_{j,k-1}^m}{\Delta\xi^2}\\&\quad+\mathcal{B}\frac{\psi_{j+1,k+1}^m-\psi_{j+1,k-1}^m-\psi_{j-1,k+1}^m+\psi_{j-1,k-1}^m}{2\Delta\xi\Delta\eta}. \quad (22)\end{aligned}$$

The obtained tri-diagonal systems of algebraic equations are solved using the well known Thomas algorithm for each (constant j) in the η-direction. The successive over-relaxation scheme is used and the relaxation parameter is chosen as 1.3 for the grid size 800×50.

The main difficulty with the stream function–vorticity formulation is to derive the boundary conditions for the vorticity. In our present computation, we obtain a second-order accurate formula for wall vorticity from the equation represented by stream function assuming the known values of the stream function. The vorticity at the walls is given by

$$\begin{aligned}\omega(\xi,0)&=-2(\mathcal{B}^2+\mathcal{G}^2)\left(\frac{\psi(\xi,\Delta\eta)-\psi(\xi,0)}{\Delta\eta^2}\right),\\\omega(\xi,1)&=-2(\mathcal{B}^2+\mathcal{G}^2)\left(\frac{\psi(\xi,1-\Delta\eta)-\psi(\xi,1)}{\Delta\eta^2}\right). \quad (23)\end{aligned}$$

This formula involves the values $\psi(\xi,\Delta\eta)$ and $\psi(\xi,(1-\Delta\eta))$ which are obtained from the coupling between ω at the

boundary and ψ in the domain. This necessitates the evaluation of ψ at the previous iteration level.

The momentum equation is now written in two half time-steps with one spatial variable implicit in one half time-step and the other spatial variable implicit in the other half time-step. Thus each half step involves the direct solution of a tri-diagonal system. During the first half time-step, the value of the vorticity ω is known at time level m and unknown at $(m+1/2)$. These unknown values $\omega_{j,k}^{m+1/2}$ are associated with the η-direction (i.e. for η implicit and ξ explicit). The discretized version of the momentum equation is given by

$$P(k)\omega_{j,k-1}^{m+1/2}+Q(k)\omega_{j,k}^{m+1/2}+R(k)\omega_{j,k+1}^{m+1/2}=S(k), \quad (24)$$

where $P(k)$, $Q(k)$, $R(k)$, and $S(k)$ are given by

$$\begin{aligned}
P(k) &= -\frac{1}{2\Delta\eta}(v\mathcal{G}-u\mathcal{B})-\frac{1}{2Re\Delta\eta}(\mathcal{A}-2\mathcal{B}\mathcal{H})-\frac{(\mathcal{B}^2+\mathcal{G}^2)}{Re\Delta\eta^2},\\
Q(k) &= \frac{2}{\Delta t}+\frac{2(\mathcal{B}^2+\mathcal{G}^2)}{Re\Delta\eta^2},\\
R(k) &= \frac{1}{2\Delta\eta}(v\mathcal{G}-u\mathcal{B})+\frac{1}{2Re\Delta\eta}(\mathcal{A}-2\mathcal{B}\mathcal{H})-\frac{(\mathcal{B}^2+\mathcal{G}^2)}{Re\Delta\eta^2},\\
S(k) &= \frac{2}{\Delta t}\omega_{j,k}^{m}-u\left(\frac{\omega_{j+1,k}^{m}-\omega_{j-1,k}^{m}}{2\Delta\xi}\right)\\
&\quad+\frac{1}{Re}\left\{\left(\frac{\omega_{j+1,k}^{m}-2\omega_{j,k}^{m}+\omega_{j-1,k}^{m}}{\Delta\xi^2}\right)\right.\\
&\quad\left.-\mathcal{B}\left(\frac{\omega_{j+1,k+1}^{m}-\omega_{j+1,k-1}^{m}-\omega_{j-1,k+1}^{m}+\omega_{j-1,k-1}^{m}}{2\Delta\xi\Delta\eta}\right)\right\}\\
&\quad+\frac{M^2\mathcal{G}^2}{Re}\left(\frac{\psi_{j,k+1}-2\psi_{j,k}+\psi_{j,k-1}}{\Delta\eta^2}\right). \quad (25)
\end{aligned}$$

Equation (24) is a tri-diagonal system of algebraic equations and is solved using the Thomas algorithm.

To advance the next half-step with the ξ-direction (i.e. ξ implicit and η explicit), the following set of equations is solved for the unknown values of $\omega_{j,k}^{m+1}$ using the known intermediate values obtained in the previous half-level as

$$P(j)\omega_{j-1,k}^{m+1}+Q(j)\omega_{j,k}^{m+1}+R(j)\omega_{j+1,k}^{m+1}=S(j), \quad (26)$$

where the quantities $P(j)$, $Q(j)$, $R(j)$, and $S(j)$ are given by

$$\begin{aligned}
P(j) &= -\frac{u}{2\Delta\xi}-\frac{1}{Re\Delta\xi^2}, \quad Q(j)=\frac{2}{\Delta t}+\frac{2}{Re\Delta\xi^2},\\
R(j) &= \frac{u}{2\Delta\xi}-\frac{1}{Re\Delta\xi^2},\\
S(j) &= \frac{2}{\Delta t}\omega_{j,k}^{m+1/2}+\left(v\mathcal{G}-u\mathcal{B}+\frac{(\mathcal{A}-2\mathcal{B}\mathcal{H})}{Re}\right)\\
&\quad\times\left(\frac{\omega_{j,k+1}^{m+1/2}-\omega_{j,k-1}^{m+1/2}}{2\Delta\eta}\right)\\
&\quad+\left(\mathcal{B}^2+\mathcal{G}^2\right)\left(\frac{\omega_{j,k+1}^{m+1/2}-2\omega_{j,k}^{m+1/2}+\omega_{j,k-1}^{m+1/2}}{Re\Delta\eta^2}\right)\\
&\quad-\mathcal{B}\left(\frac{\omega_{j+1,k+1}^{m+1/2}-\omega_{j+1,k-1}^{m+1/2}-\omega_{j-1,k+1}^{m+1/2}+\omega_{j-1,k-1}^{m+1/2}}{2Re\Delta\xi\Delta\eta}\right)\\
&\quad+\frac{M^2\mathcal{G}}{Re}\left(\frac{\psi_{j,k+1}-2\psi_{j,k}+\psi_{j,k-1}}{\Delta\eta^2}\right). \quad (27)
\end{aligned}$$

Solving the systems (26), the vorticities at the $(m+1)$th level are obtained in the computational plane.

The detailed derivation of the numerical scheme can be obtained from Ref. [19].

Some restrictions on time-step Δt for numerical stability of the scheme are required. The first restriction, known as the CFL (Courant, Friedrichs and Lewy) condition, is given by

$$\Delta t_1 \le \mathrm{Min}\left[\frac{\Delta\xi}{|u|},\frac{\Delta\eta}{|v|}\right]_{(j,k)}.$$

The second restriction relates to viscous effects and is given by

$$\Delta t_2 \le \mathrm{Min}\left[\frac{Re}{2}\frac{\Delta\xi^2\Delta\eta^2}{(\Delta\xi^2+\Delta\eta^2)}\right]_{(j,k)}.$$

Finally, the time step Δt is chosen using the above relations as

$$\Delta t=\beta\mathrm{Min}\left[\Delta t_1,\Delta t_2\right],$$

where the minimum is taken in the global sense.

5. Results and discussion

We made a grid independence test for verification of the accuracy of the results by taking the grid sizes 300×20, 600×40, and 1200×80. The accuracy of data is shown in Table 1 for the flow Reynolds number $Re=700$ and for the values of Hartmann numbers $M=0$, 2. The results obtained by taking the grid distributions 600×40 and 1200×80 agree well. Finally, we chose the grid size as 800×50 for all computations in this study. The validation of the method was achieved by comparing our results with the results obtained by Layek and Midya[33] and is presented in Table 2 for the Reynolds number $Re=600$. The results are found to be in excellent agreement.

Table 1. Primary separation lengths at the upper and lower walls for $Re=700$ for $M=0$ and 2.

	Case I $M=0$		Case II $M=2$	
Grid	Upper wall	Lower wall	Upper wall	Lower wall
300×20	14.724	16.953	7.272	7.684
600×40	14.662	17.081	7.161	7.833
1200×80	14.650	17.100	7.150	7.850

Table 2. Results of u-velocity for a long straight channel at $Re = 600$ for $M = 0$ and $M = 2$.

	Case I $M = 0$							
Property	$y \to 0$	0.1	0.3	0.5	0.7	0.9	1	Scheme
$u = y - y^2$	0	0.09	0.21	0.25	0.21	0.09	0	exact
u	0	0.089947	0.2099	0.2498	0.2099	0.089947	0	Layek & Midya[33]
u	0	0.08999	0.2098	0.2498	0.2098	0.08999	0	obtained in present numerical scheme
	Case II $M = 2$							
u	0	0.09452	0.2123	0.2496	0.2123	0.09452	0	obtained in present numerical scheme

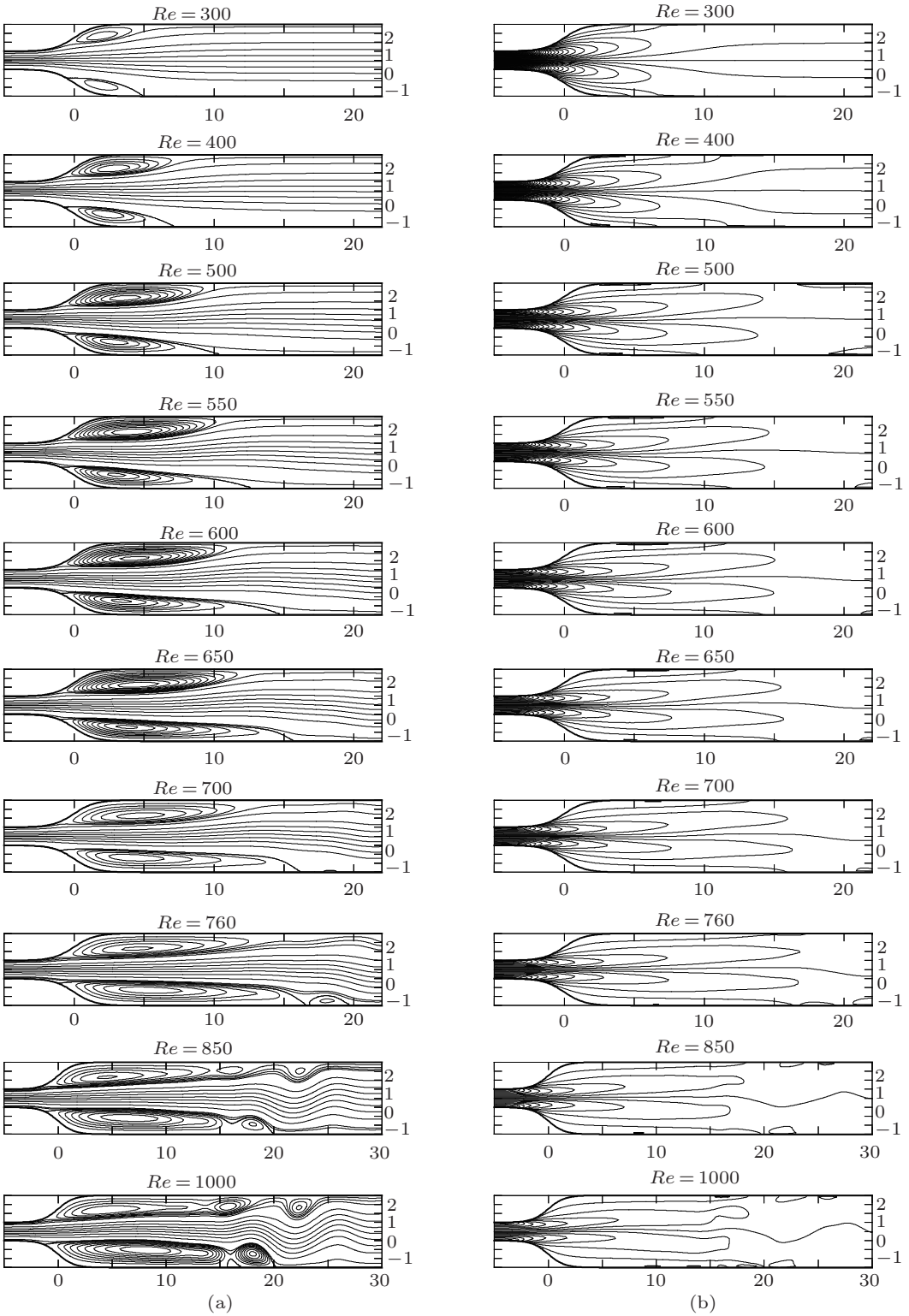


Fig. 2. Pattern of streamlines (a) and vorticity contours (b) for different Reynolds numbers (Re) in a smoothly expanding channel for the electrically non-conducting fluid flows.

First, we give our attention to the electrically non-conducting fluid flowing in a smoothly expanding channel. The flow analysis in the smooth expansion geometry is useful for many practical devices. The pattern of streamlines and the vorticity contours for $M = 0$ for several values of the Reynolds number (Re) have been exhibited in Figs. 2(a) and 2(b). Depending upon the flow Reynolds number, recirculation regions of different sizes and strengths attached to the upper and lower walls are observed. It is noticed from Fig. 2(a) that the reattachment lengths increase behind the smooth expansion with increasing values of the Reynolds numbers. However, the length of separation at the lower wall is much larger than the length of separation at the upper wall. The reason for this phenomenon is that the flow undergoes first bifurcation leading to an asymmetric pattern of flow. A secondary separation region is developed first at the Reynolds number $Re = 700$ approximately at the lower wall of the channel. The corresponding vorticity contours are shown in Fig. 2(b). The vorticities are formed and concentrated in the expanded region of the channel. It is observed that the recirculating bubbles are not symmetric about the center line of the channel. When the Reynolds number exceeds the value of approximately 300, the flow field first undergoes symmetry-breaking bifurcation.

In the case of an electrically conducting liquid metal, electromagnetic force alters the flow field drastically. This magnetic force is proportional to the square of the externally applied magnetic field (B_0) in the induction-less situation. A flow bifurcation diagram is presented in Fig. 3 for both the cases (electrically non-conducting and conducting for $M = 0$ and 2). The measure of the flow asymmetry is calculated by the parameter $\mathrm{DX} = (X_2 - X_1)$ (see Ref. [6]), where X_1 and X_2 are the lengths of primary separation regions of lower and upper walls of the channel, respectively. It is observed that the value of DX is zero for symmetric flow and non-zero, with opposite signs, for asymmetric flow. The upper branch in Fig. 3 corresponds to flow attaching first to the lower wall and, conversely, the lower branch corresponds to the flow attaching to the upper wall. The symmetric flow about the centerline of the channel is maintained up to $Re = 300$. However, in the case of an electrically conducting fluid in the presence of magnetic field B_0 the flow remains symmetric up to $Re = 475$ for $M = 2$. Table 3 presents two cases: (i) $M = 0$ and (ii) $M = 2$ for several values of the Reynolds number (Re). This also gives the lengths of separation bubbles formed at the lower and upper walls of the channel for two cases. The important point is to note that the asymmetric flow field can be made symmetric by applying suitable magnetic field. In order to elucidate the effects of the Hartmann number M $(= B_0 h\sqrt{\sigma/\rho\upsilon})$, the lengths of recirculation regions developed due to smooth expanded geometry have been presented in Figs. 4(a)–4(b). The lengths of recirculation regions decrease with increasing values of M for both walls. This happens due to the increase of Lorentz force with the increase of the magnetic field B_0.

Table 3. Primary separation lengths at the upper and lower walls for different values of Re in the presence and absence of magnetic field.

	$M = 0$ (pure fluid)		$M = 2$ (conducting fluid flow)	
Re	Upper wall	Lower wall	Upper wall	Lower wall
200	3.4	3.4	–	–
250	4.7	4.7	–	–
298	5.8	5.95	–	–
300	5.85	6.1	–	–
400	8.05	8.95	–	–
450	9.45	10.2	4.1	4.1
475	10.35	10.75	4.45	4.45
480	10.42	10.87	4.50	4.54
500	11.25	11.30	4.70	4.85
550	12.1	13.55	5.40	5.55
600	12.9	15.6	6.0	6.3
650	13.75	16.6	6.55	7.1
670	14.15	16.8	6.75	7.4
680	14.3	16.9	6.85	7.6
700	14.65	17.10	7.15	7.85

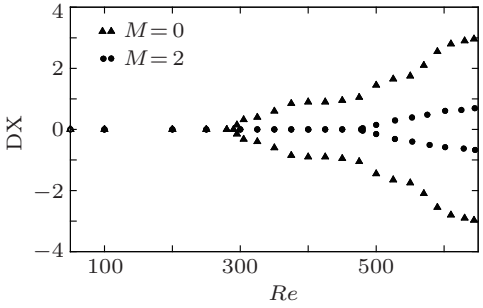


Fig. 3. Flow bifurcation diagram in a smoothly expanding channel for different values of magnetic parameter M.

The estimation of wall shear stresses at upper and lower walls is important in flow devices. In particular, we have drawn wall shear stress curves for both the walls for different values of the Hartmann number, say $M = 0$, 2, 3, 4 at the Reynolds number $Re = 700$ (see Figs. 5(a) and 5(b)). The negative values of shear stress correspond to the flow separation region at the upper wall whereas the positive values of the shear stress corresponds to the separation region at the lower wall. The lengths of the separation regions for both walls decrease with increasing values of the Hartmann number M. The retarding Lorentz force acts to suppress the flow, giving a reduction of flow separation lengths. It is also noted that for $Re = 700$ a secondary separation region is developed at the lower wall in the absence of the magnetic field. In the case of an electrically conducting fluid the secondary flow separation region is diminished in length with increasing M (see Fig. 5(b)). The Hartmann boundary layer which is formed near the wall becomes thinner, resulting in an increase in the velocity gradient near the walls. In the case of the Hartmann flow problem the thickness of the boundary layer is of order $(1/M)$ for high value of M (the velocity differential is confined only in a thin layer attached to the channel walls and the rest of it becomes practically constant). The wall shear stress increases with increase of Hartmann number.

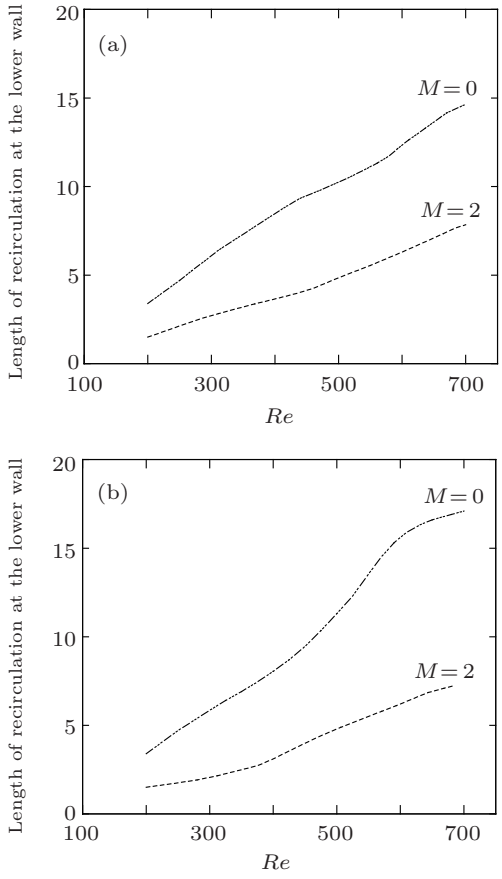


Fig. 4. (a) Recirculating length at the upper wall in a smooth expanded channel for different values of M. (b) Recirculating length at the lower wall in a smoothly expanding channel for different values of M.

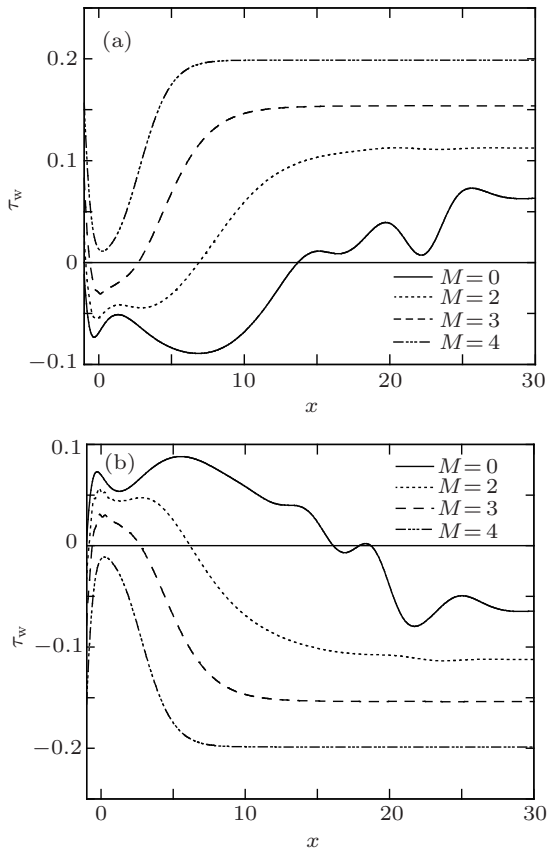


Fig. 5. (a) Distribution of wall shear stress (τ_w) at the upper wall for $Re = 700$ for several values of M in a smoothly expanding channel. (b) Distribution of wall shear stress (τ_w) at the lower wall for $Re = 700$ for several values of M in a smoothly expanding channel.

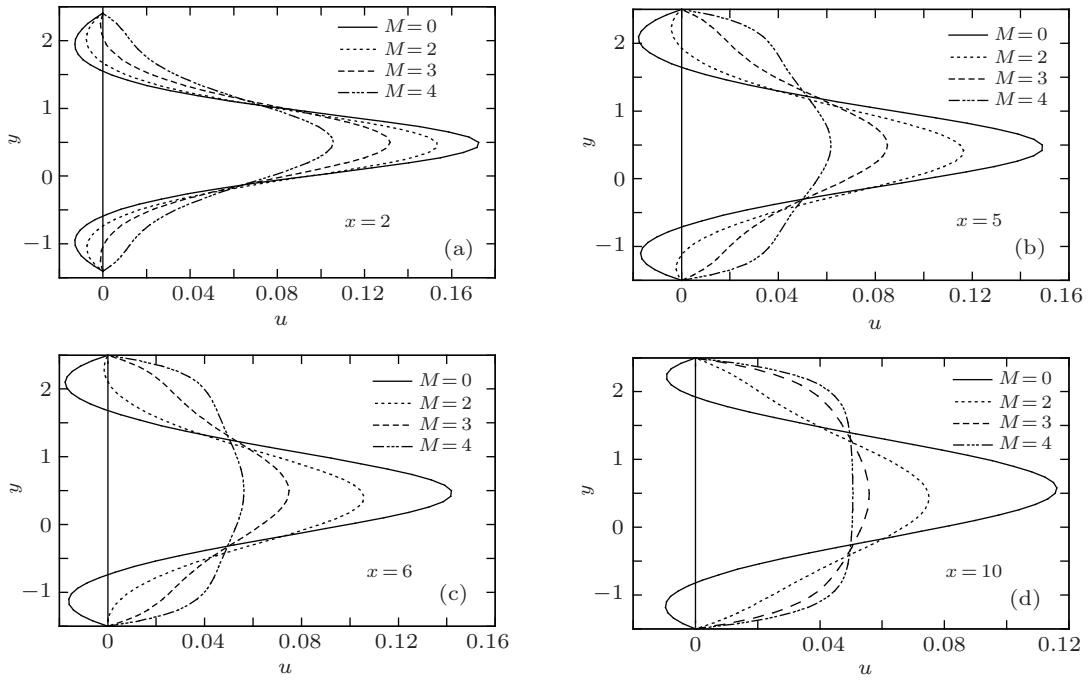


Fig. 6. u-velocity distribution versus y in a smoothly expanding channel at different axial positions for $Re = 700$ and different values of the Hartmann number (M). (a) $x = 2$, (b) $x = 5$, (c) $x = 6$, and (d) $x = 10$.

The velocity profiles at different axial positions $x = 2$, 5, 6, and 10 have been displayed in Fig. 6 for $M = 0$, 2, 3, and 4 and for $Re = 700$. These figures reveal that the axial velocity u becomes flattened and moves towards the wall as the magnetic field strength M increases (the same as Hartmann flow). The flow is confined near the wall for large values of M as depicted

in the figures.

In Fig. 7, the u-component of velocity is presented at different axial positions for $Re = 760$ and for different values of $M = 0$, 2, 3. It can be seen that at $M = 0$ the u-velocity profile tends to separate in the expanded region of the channel, and this is gradually redeveloped with increasing values of M.

The pattern of streamlines and the corresponding vorticity contours for different values of Hartmann number for the Reynolds number $Re = 760$ are displayed in Figs. 8(a)–8(b). The recirculation regions of different sizes and strengths attached to the upper and lower walls of the expanded channel are shown. A third recirculation region appears at the lower wall first when $M = 0$. However, the length of the recirculation region is decreased with increasing values of the Hartmann number. The vortices formed near the expanded region are suppressed with increasing values of M. As discussed in the earlier section, the suppression of vortices made the boundary layer thinner.

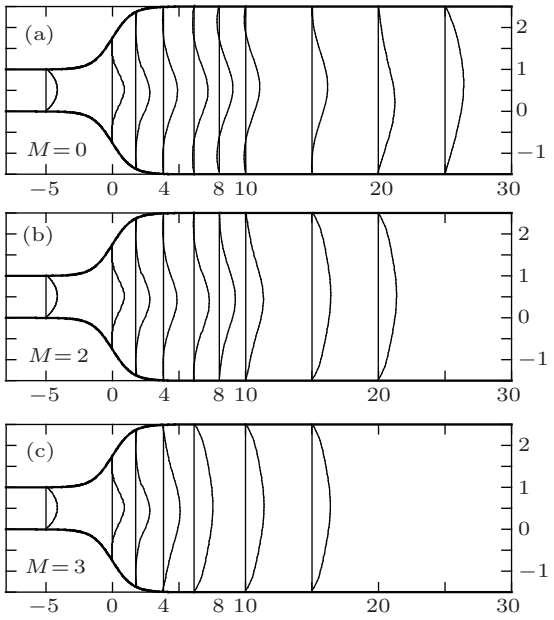


Fig. 7. u-velocity profiles at different axial positions in a smooth expanded channel for different Hartmann numbers (M) for the Reynolds number $Re = 760$. (a) $M = 0$, (b) $M = 2$, (c) $M = 3$.

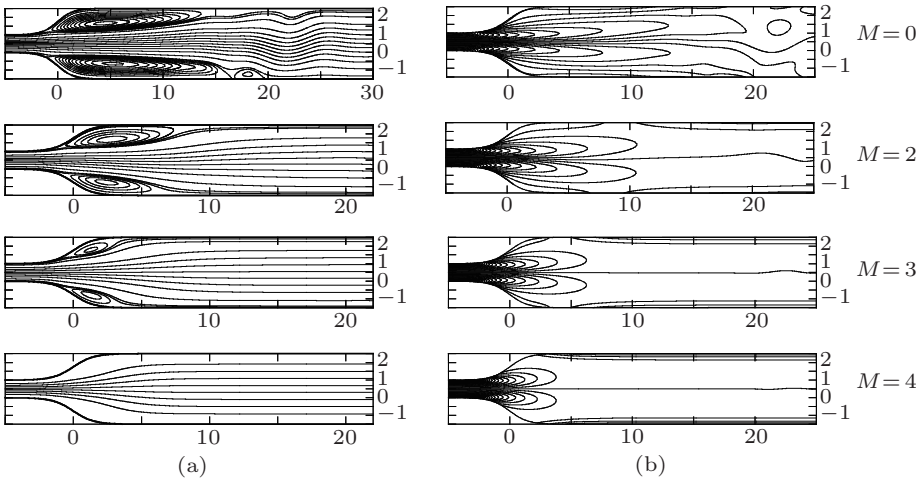


Fig. 8. Pattern of (a) streamlines and (b) vorticity contours for different values of Hartmann number (M) in a smoothly expanding channel for $Re = 760$, displaying separating bubbles formed near the expanded region.

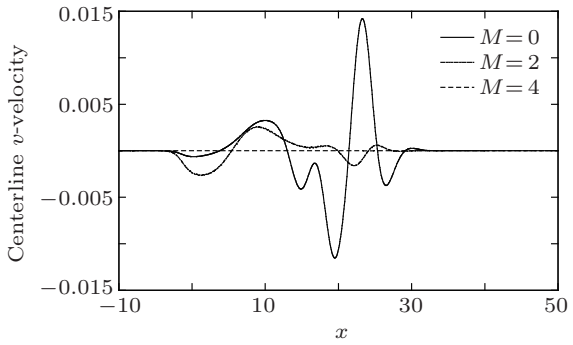


Fig. 9. Centerline v-velocity for different Hartmann numbers (M) in a smoothly expanding channel for $Re = 760$.

We have also drawn the centerline v-velocity of the flow field. The centerline v-velocity component becomes zero when the flow is symmetric about the centerline ($y = 0$) of the channel. One can estimate the non-zero values of v-velocity component as a measure of flow asymmetry. Figure 9 shows the variation of the centerline v-velocity for $Re = 760$ for different values of $M = 0$, 2, 4. It indicates that the centerline v-velocity becomes oscillatory in the expanded regions of the channel, and the oscillation decreases with increasing values of M. This indicates that the expanded region is the source of vorticity and instigates flow asymmetry.

Next, we measure the flow asymmetry by calculating the root mean square (RMS) of v-velocity component at the channel centerline. The RMS of v-velocities at the centerline against Reynolds number has been plotted in Fig. 10 for several values of M. The critical value of Reynolds number

Re_c is approximately 298 for non-conducting fluid, that is, $M = 0$. It is shown that the flow remains symmetric up to the Reynolds number Re of approximately 475 for $M = 2$. The results demonstrate that the magnetic field can be used for the suppression of flow separation and bifurcation.

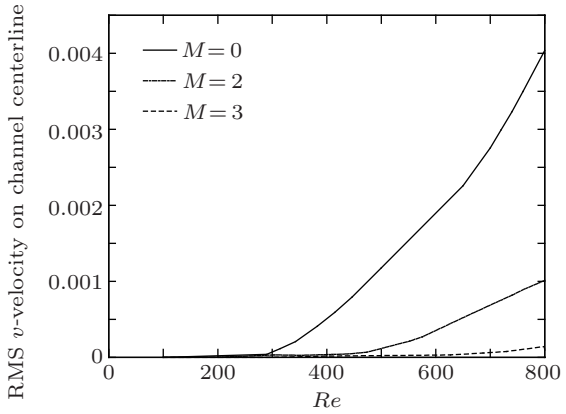


Fig. 10. Root mean square velocity (RMS) v-velocity on channel centerline for different Hartmann numbers (M) in a smooth expanded channel for $Re = 760$.

6. Conclusions

In summary, the effects of transverse uniform externally applied magnetic field on flow separation regions formed behind the smoothly expanding channel and flow bifurcation for an electrically conducting fluid is investigated. The induction-free case is considered and this is valid only for flows of liquid metals. The MHD non-linear governing equations under MHD approximations (applicable for usual fluid motion) are solved using the finite-difference technique. The following are the main observations made from this study.

(i) The smoothness of geometry is an important controlling factor for flow separation and flow bifurcation. In the case of a suddenly expanding channel (1:4 aspect ratio) the critical value of Reynolds number for bifurcation is 36, whereas for the smooth expansion considered in this work its value becomes approximately 298, a very high value compared to sudden expansion.

(ii) The flow field alters significantly due to the developed electro-magnetic force for the motion of an electrically conducting fluid in the presence of magnetic field. For example, the critical value for flow bifurcation is 475 for the Hartmann number $M = 2$ (supercritical bifurcation). The flow separation lengths at the lower and upper walls are significantly reduced. The quantitative analysis is made by presenting data in tables.

(iii) The length of separation at the lower wall of the symmetric expanded channel is larger than that of the upper wall after the critical value of the Reynolds number.

(iv) A third recirculation region appears at the lower wall for $Re = 700$ and $M = 0$. It is interesting to note that all separating regions appearing behind the expansion were suppressed completely for $M = 4$.

(v) The separation and bifurcation occur earlier for the case of a suddenly expanding channel.

From this work one can make a comparison study to analyze the flow fields in suddenly and smoothly expanding channels. The results obtained in this study may be useful to the scientists working in this area.

References

[1] Armaly B F, Durst F, Pereira J C F and Schonung B 1983 *J. Fluid Mech.* **127** 473
[2] Durst F, Melling A and Whitelaw J H 1974 *J. Fluid Mech.* **64** 111
[3] Durst F, Pereira J C and Tropea C 1993 *J. Fluid Mech.* **248** 567
[4] Cherdron W, Durst F and Whitelaw J H 1978 *J. Fluid Mech.* **84** 13
[5] Fearn R M, Mullin T and Cliffe K A 1990 *J. Fluid Mech.* **211** 595
[6] Drikakis D 1997 *Phys. Fluid.* **9** 76
[7] Wille R and Fernholz H 1965 *J. Fluid Mech.* **23** 801
[8] Sobey I J and Drazin P G 1986 *J. Fluid Mech.* **171** 263
[9] Borgas M S and Pedley T J 1990 *J. Fluid Mech.* **214** 229
[10] Shapira M, Degani D and Weihs D 1990 *Comput. Fluids* **18** 239
[11] Rocha G N, Poole R J and Oliveira P J 2007 *J. Non-Newtonian Fluid Mech.* **141** 1
[12] Gad-el-Hak M and Bushnell D M 1991 *J. Fluids Engg.* **113** 5
[13] Bhattacharyya K and Layek G C 2010 *Chem. Engg. Commun.* **197** 1527
[14] Bhattacharyya K, Mukhopadhyay S and Layek G C 2011 *Chin. Phys. Lett.* **28** 024701
[15] Bhattacharyya K, Mukhopadhyay S and Layek G C 2012 *Chem. Engg. Commun.* **199** 368
[16] Nadeem S and Haq R U 2014 *J. Comput. Theor. Nanoscience* **11** 32
[17] Nadeem S, Haq R U and Akbar N S 2014 *Nanotechnology* **13** 109
[18] Midya C, Layek G C, Gupta A S and Mahapatra T R 2003 *J. Fluids Engg.* **125** 952
[19] Bandyopadhyay S and Layek G C 2012 *Commun. Nonlinear Sci. Numer. Simult.* **17** 2434
[20] Layek G C and Midya C 2007 *Magnetohydrodynamics* **4** 3
[21] Holstein P A, Delettrez J, Skupsky S and Matte J P 1986 *J. Appl. Phys.* **60** 2296
[22] Jungclaus G 1960 *Rev. Mod. Phys.* **32** 823
[23] Layek G C, Kryzhevich S G, Gupta A S and Reza M 2013 *Z. Angew. Math. Phys.* **64** 123
[24] Nadeem S, Haq R U and Lee C 2012 *Scientia Iranica.* **19** 1550
[25] Nadeem S, Haq R U, Akbar N S and Khan Z H 2013 *Alexandria Engg. J.* **52** 577
[26] Akbar N S, Nadeem S, Haq R U and Khan Z H 2013 *Chin. J. Aeronautics* **26** 1389
[27] Nadeem S, Haq R U and Khan Z H 2014 *J. Taiwan Institute Chem. Eng.* **45** 121
[28] Bhattacharyya K and Layek G C 2012 *Meccanica* **47** 1043
[29] Bhattacharyya K and Layek G C 2014 *Phys. Res. Int.* **2014** 592536
[30] Zikanov O and Thess A 1998 *J. Fluid Mech.* **358** 299
[31] Cowling T G 1957 *Magnetohydrodynamics* (New York: John Wiley and Sons)
[32] Pedrizzetti G 1996 *J. Fluid Mech.* **310** 89
[33] Layek G C and Midya C 2007 *Commun. Nonlinear Sci. Numer. Simult.* **12** 745
[34] Peyret R and Taylor T D *Computational Methods for Fluid Flow* (Berlin, Heidelberg: Springer-Verlag)